STABILITY ANALYSIS OF THE 4TH ORDER RUNGE KUTTA METHOD IN APPLICATION TO COLLOIDAL PARTICLE INTERACTIONS

BY

SINDHUJA REDDY VELGALA

THESIS

Submitted in partial fulfillment of the requirements
for the degree of Master of Science in Chemical Engineering
in the Graduate College of the
University of Illinois at Urbana-Champaign, 2014

Urbana, Illinois

Adviser:

Professor Jonathan Higdon

Abstract

Colloidal particles have a wide range of industrial applications. This study is focused on the application to microstructured materials and the impact of external compressive forces on particles. Currently, in the large throughput manufacturing of microstructured materials, problems such as cracking are caused by these external forces. Numerical methods can be used to generate particle positions and obtain a better understanding of particle interactions under different conditions. The aim of this study was to obtain a better understanding of the stability limits of using the 4^{th} order Runge Kutta method. By introducing the external forces as auxiliary functions, we were able to generate exact analytic solutions satisfying arbitrary hydrodynamic and interaction forces. This allowed rigorous comparison of the theoretical stability limits and the observed stability limits on time step. We found excellent agreement with the predicted and observed results.

TABLE OF CONTENTS

CHAPTER 1

INTRODUCTION

1.1 Overview

Applications

Colloidal suspensions refer to multiphase materials consisting of a fluid solvent and particles dispersed within a suspension. These particles could range in size from a few micrometers to nanometers. Suspensions could also consist of more than one type of particle. Many items that we use daily are colloidal suspensions and studying them in order to understand particle behavior under different conditions is vital. Applications of colloidal suspensions range from personal care items such as shampoos, toothpastes to food items such as milk. Coating materials such as paints and sprays also work on the basis of colloidal physics.

More recently, the focus on the use of colloidal suspensions in the manufacture of novel microstructured materials has increased. Batteries, electrodes and many other materials used in devices such as semiconductor chips, catalytic converters, etc. consist of colloidal suspensions. Colloidal properties are manipulated in order to cater to each of the above applications (Larson, 1999).

Processing operations

Independent of the application, the processing steps that are involved in the manufacture of colloidal suspensions are similar. There are four main steps. The analogy between the paper manufacture process and the electrode manufacture process is illustrated in Figures 1.1 and 1.2. The first step is the mixing of the components used to make the material. This involves mixing different types of solids in a fluid suspension, using mechanical agitation. As illustrated by Figure 1.2a, this is the step where the materials used to make the electrodes are mixed. One challenge that is faced in this step is to prevent the breakup of particles, while encouraging the break-up of clusters in order to achieve uniform mixing. The next step is the coating of the material. This is where a particulate suspension is applied in a thin uniform layer on a substrate to form a uniform particle coating. As shown in

Figure 1.1, in the case of paper processing, this is the step where the pulp material is sprayed onto a moving belt of mesh screening. Figure 1.2b shows the substrate being coated with the electrode material. A challenge in this step is to ensure that the coating is even across the surface of the material. Next, the material is consolidated or compressed in order to remove some of the liquid. Consolidation is done by passing the suspension through rollers, as shown in Figure 1.1 and 1.2c. Finally, the material is dried to achieve the end solid product. Drying is generally performed by passing the material through heated chambers, leading to evaporation of the solvent. In these two steps, compressive forces that act during consolidation and drying result in the formation of cracks. It is important to manipulate processing conditions, such that the problems associated with each step do not occur.

The processing steps involved in the manufacture of paper and the manufacture of electrodes are illustrated below.

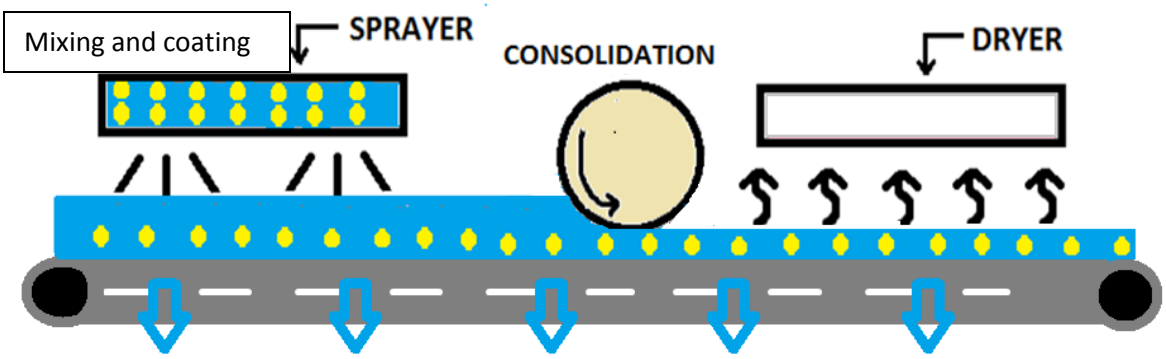

Figure 1.1 Paper Manufacturing Process

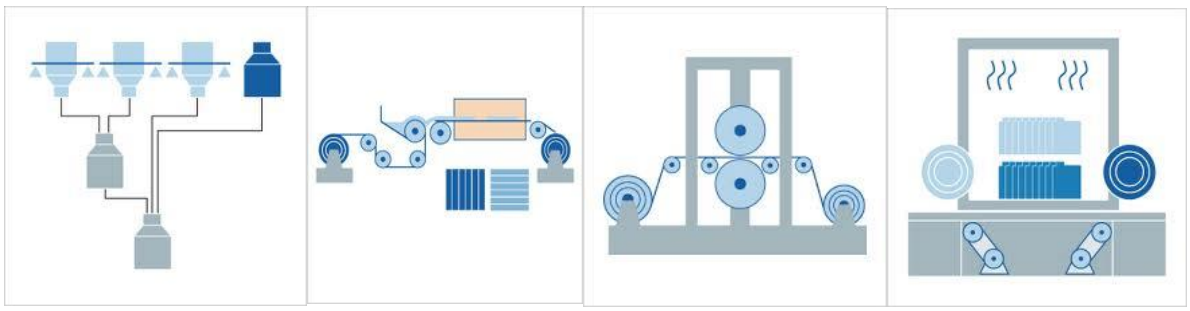

(a) Mixing (b) Coating (c) Consolidation (d) Drying

Figure 1.2 Electrode Manufacturing Process (Siemens)

Despite the similarity of processing methods for most colloidal suspensions, there are different types of requirements that need to be met during high throughput manufacturing. In the case of paper manufacture, it is not crucial that complete homogeneity be achieved while mixing, or that the processing conditions for consolidation and drying be monitored carefully in order to prevent cracks. However, for microstructured materials such as electrodes, these issues are much more relevant. It is crucial to achieve a uniform distribution of particles and to manipulate of properties in order to prevent cracks. Given the number of applications of colloidal suspensions, it is important to note that colloidal properties must be manipulated to cater to each of these applications. Some such colloidal properties will be explained in more detail in the next section.

1.2 Properties

Colloidal dispersions have complicated dynamics and exhibit many different phase transitions and rheological properties.

Stability

Colloidal instability results from the thermodynamic drive to reduce surface energy through the aggregation of particles in a dispersed solution. Aggregation usually occurs spontaneously and can be exacerbated by the addition of salt or by any method that reduces repulsion between particles, such as introducing charge into the system. Aggregation is irreversible and can only be reduced by introducing repulsive forces into the system. The problem with aggregation of particles is that it leads to unevenly distributed, larger sized particles which might not work in certain applications. In addition, aggregation causes suspensions with more than one type of particle to be unevenly distributed (Larson, 1999)

Interparticle interactions

There are 3 main types of interactions that occur between colloidal particles. The first are hydrodynamic forces, which result from the motion of colloidal particles being dispersed in a viscous fluid. Next are Brownian forces, which arise from thermal fluctuations in the suspending fluid. Finally, attractive and repulsive forces can be introduced into the system through means such as polymer depletion and introduction of charge into the system.

Changes in these interparticle interactions lead to changes in the microstructure of the colloidal suspensions, thus having an impact on the rheological and mechanical properties of the systems (Russel, 1991).

Microstructure

The microstructure of a colloidal suspension refers to the spatial distribution of particles at any moment in time. Analyzing microstructures can determine several material properties, including the volume fraction of a colloidal suspension, degree of mixing, order, etc. The volume fraction of a colloidal suspension is determined by the number of colloidal molecules with respect to the amount of solvent. Concentrated solutions exhibit different properties for more dilute suspensions. The microstructure also determines whether a solution is monodispersed or polydispersed, as it displays the existence of different sizes and types of particles. The degree of mixing determines how well different types of particles are dispersed. The arrangement of particles can either be ordered or disordered, depending on whether the particles are arranged in a proper lattice structure. The pair distribution is a quantitative way to describe the microstructure. It describes the spatial positions and relationship between pairs of particles. Introducing interparticle interactions into a system can lead to changes in the microstructure of a system, which then leads to changes in the mechanical and rheological properties of the suspensions.

In order to illustrate how changes in interparticle interactions lead to changes in the microstructure, computational simulations have been conducted by Bybee and the results are as displayed in the figures below. Each box depicts the microstructure at a particular strength of attraction and repulsion. Combined, the boxes depict the evolution of the microstructure as increased strengths of attractions and repulsions are introduced into the system. Coloring of the particles goes from blue to yellow, depending on the contact number of the particles. The contact number of each particle refers to the number of particles surrounding that particle. Systems with more aggregation display more yellow colored particles, whereas systems with less aggregation display more blue colored particles. Figure 1.3 depicts 4 different microstructures, as the strength of attraction is increased from 0 KT to 7.9 KT. This simulation was conducted at a volume fraction of 0.33. As shown in Figure 1.3a when no attraction is introduced into the system, the colloidal particles are free to move and fluid-like.

In Figure 1.3b, as the attraction increases to 4.6KT, the particles temporarily attach to neighboring particles. However, the attraction is not strong enough for a strong bond to be formed. Therefore, particles quickly rise out of the attraction well and are detached. In Figure 1.3c, at an attraction of 4.7KT, there is a sudden transition to a crystal state. As attraction is increased even further, particles do not have time to rearrange themselves into a crystalline structure and are in a state of kinetic arrest. At this point, the suspension is considered to be a non-equilibrium gel. This microstructure is displayed in Figure 1.3d, at an attraction of 7.9KT (Bybee, 2009).

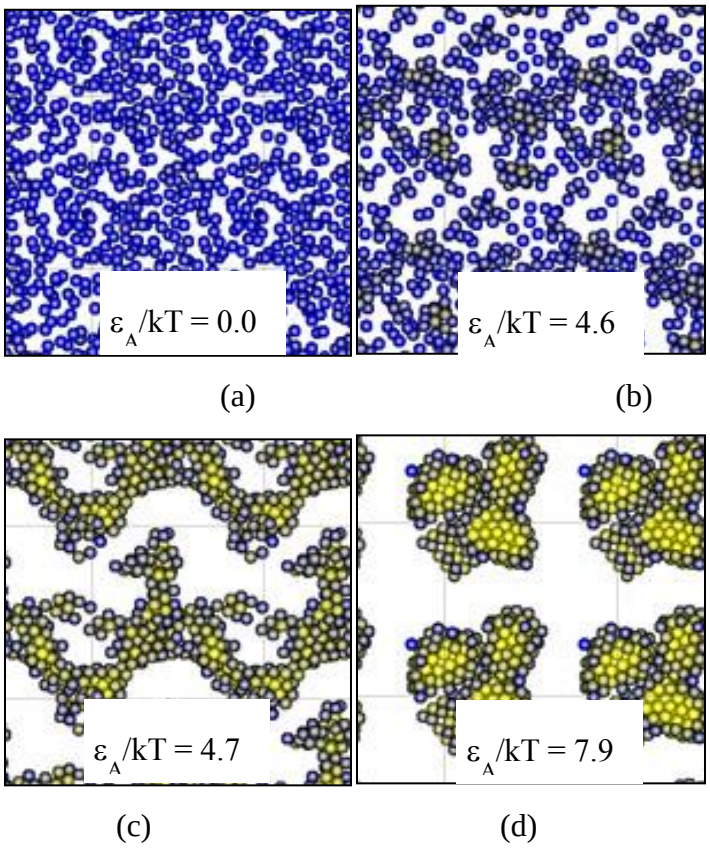

Figure 1.3 Effect of increasing strengths of attractions on the microstructure (Bybee, 2009)

Figure 1.3 was conducted under zero repulsion. Bybee also conducted studies on the microstructure, as repulsions were introduced into the system. The 2 boxes below display the microstructure at a strength of attraction of 11.8KT and the given strengths of repulsions.

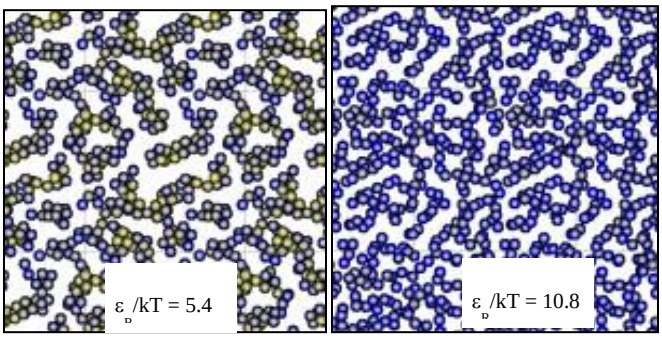

(a) (b)

Figure 1.4 Microstructure -attraction of 11.8KT and different strengths of repulsion (Bybee, 2009)

At both low and high repulsions, gels form, as long as there is strong attraction. However, the gel structures become thinner and thinner, as higher and higher repulsive forces are introduced into the system. This is illustrated in Figure 1.4, whereby thinner gel structures are formed when the strength of repulsion is increased from 5.4KT to 10.8KT. This variation in the arrangement of the particles has an impact on the mechanical properties of the material, such as yielding and cracking, as will be described in a later section.

Rheology

Rheology determines the response of a material to perturbation. Colloidal suspensions are viscoelastic, which means that they exhibit both solid-like and fluid-like properties, though not necessarily in equal proportions. It is important to characterize the rheology of a material in order to better understand its reaction to stress and therefore, predict cracks and yielding properties of the material.

In order to characterize the rheology of the materials, a rheometer is used. In the simplest cases, a shearing flow is imposed on the liquid and stresses are measured or vice-versa. In general, for solid-like suspensions, the stress grows linearly with strain until a critical value is reached. Beyond this critical value, cracking or yielding occurs. Liquid-like materials reach instantaneously steady-state viscosity values upon shearing (Larson, 1999). Many experiments have been performed in order to determine characteristics of colloidal suspensions and understand their behavior. The behavior of colloidal suspensions when

attractions are introduced into the system is slightly different. Increasing attractive forces causes the viscosity to diverge and display a large degree of shear thinning as shown in Figure 1.5a. The elastic modulus changes by several orders of magnitude with increasing attraction, and it is dependent on the volume fraction, as illustrated in Figure 1.5b. The viscosity describes the resistance to flow and the elastic modulus describes the elasticity of a material.

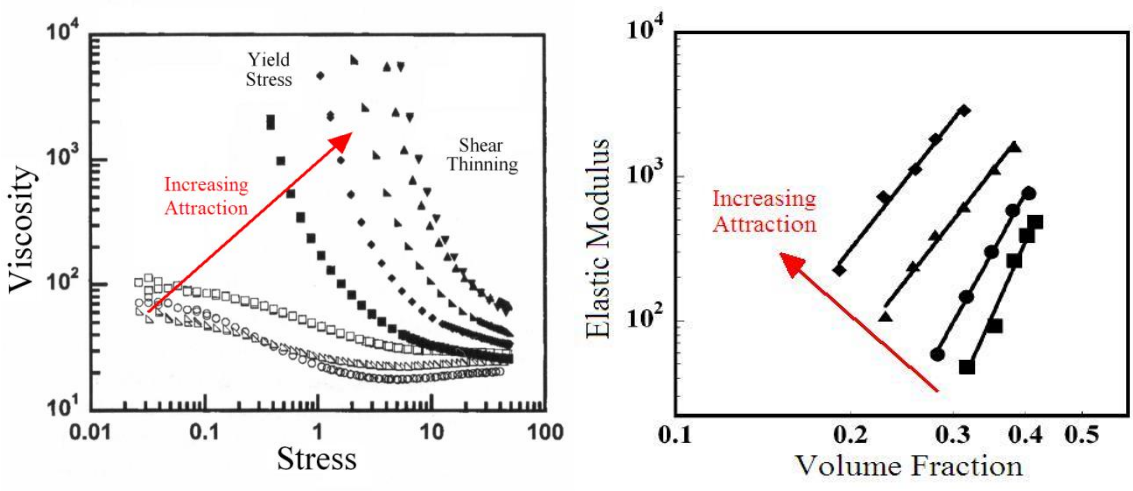

(a) (b)

Figure 1.5 Graphs displaying rheology of colloidal suspensions with increasing attraction (Gopalkrishnan, 2007) (Ramakrishnan, 2005)

Mechanical properties

It was stated previously that a change in microstructure could lead to a change in the mechanical properties of the system. Bybee also conducted simulations in order to understand the impact interparticle interactions have on the yielding behavior of materials. Figure 1.6 depicts yielding behavior at an attraction of 17.1KT and increasing strengths of repulsion.

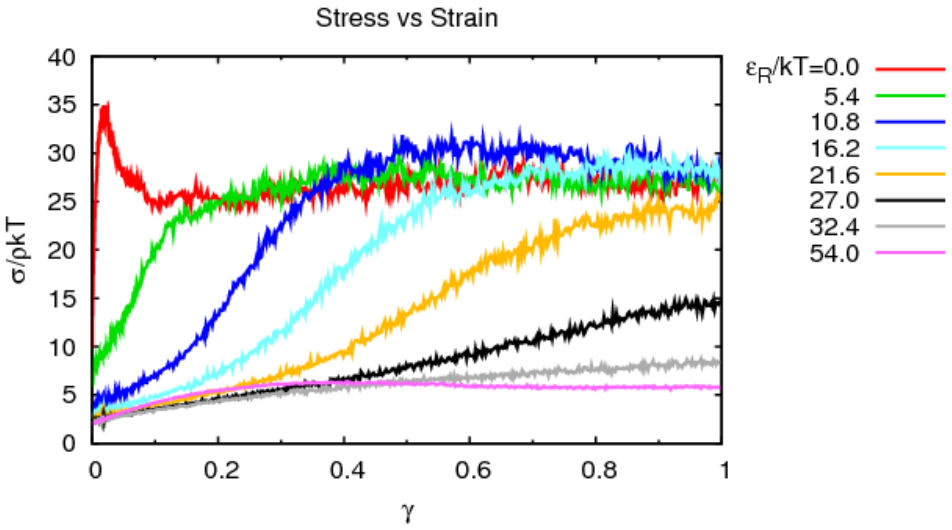

Figure 1.6 Stress vs Strain curve at different strengths of repulsions (Bybee, 2009)

In materials that are purely attractive, yielding occurs at very small strains. In Figure 1.6, the red line shows the change in the stress of the material as strain is introduced into the system, at zero repulsion. The instantaneous increase in stress shows that the material has cracked under the strain. This stress then decreases after the material breaks and tends off towards a steady state. This phenomenon is due to the fact that at low repulsions, the structures are thick, inflexible and brittle. As the strength of repulsion is increased further, structures are thinner, more flexible and softer, as illustrated in Figure 1.3 above. Therefore, at large strengths of repulsions such as 32.4 KT and 54.0KT, no matter how much strain is introduced into the system, there is negligible impact on the stress. The impact that changes in interparticle interactions has on microstructure and thus, the material and rheological properties has been explained in detail. Analyzing the microstructure for different parameters is vital to predicting how the material reacts under different processing conditions.

Any of the process steps could lead to an uneven distribution of particles, which will cause problems such as cracking. As can be seen from Figure 1.7 below, an uneven stress distribution leads to the stress propagating through uneven lengths of chains of molecules. This leads to cracks in latter processing steps. Predicting the microstructure early on can help prevent cracks.

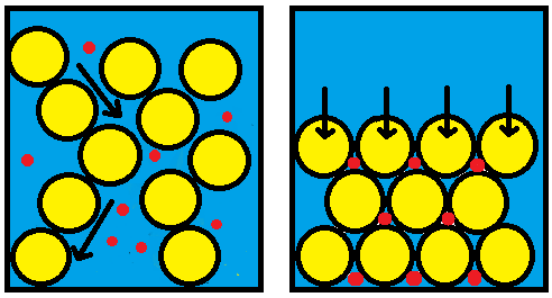

Figure 1.7 Uneven stress distribution vs. even stress distribution

In addition to an even stress distribution, it is also important to maintain a uniform particle distribution and ensure that homogeneity is achieved during steps such as mixing. For materials such as electrodes, a low distribution of conducting particles on one side would mean that the electrode would lose its conducting property.

1.3 Experiments

Experiments depicting specific process steps have also been conducted. Two of the most challenging process steps in the production of microstructured materials are the consolidation step and the drying step. In order to correctly mimic these steps in experiments, it is important to understand some of the theory associated with them.

Consolidation

Consolidation, as described above, is a fundamental unit operation involving the partial or complete removal of fluid from a colloidal suspension. There are different ways to remove the fluid, including mechanical compression, osmotic consolidation, sedimentation and centrifugation. Sedimentation and centrifugation are slow processes and are commonly used for the consolidation of larger particles. Osmotic consolidation and mechanical consolidation are used for smaller sized particles. Studies conducted on mechanical consolidation and osmotic consolidation have been shown to exhibit similar results in some cases and in others, osmotic consolidation has led to denser suspensions (Miller, 1996). There are 2 aspects involved in mechanical consolidation- the viscous flow and the elastic response. The viscous flow is associated with the permeability in porous media, or how the liquid flows throw the particles. The elastic response has to do with the compression of the solid network and the

breaking and formation of bonds. In mechanical compression, the weight of the load is determined such that the force on the piston exceeds the sum of hydrodynamic, solid matrix and interparticle forces. Small loads can be sustained elastically. The speed of compression is also a parameter that needs to be adjusted. At a high compression rate, the fluid rushes through spaces between the particles and causes a lot of perturbation and movement of the colloids. Therefore, hydrodynamic forces are essential and stress is distributed between all 3 components. At low compression rates, hydrodynamic forces are negligible and stress distribution is between the solid matrix and the interparticle interactions. Studies have shown that non-homogeneity in particle suspensions causes different responses to the static load. In order to study compressive effects on heterogeneous suspension, preparation of samples and level of shearing is crucial (Channel, 1997).

Drying

Drying completely removes all fluid from the colloidal suspension, leaving behind a solid product. Various studies have been performed on the drying process, including analyses of crack formations. During the drying process, it is important to consider the dimensions of the final product as well. In addition to consolidation forces, capillary forces are also faced by the colloidal suspension. These forces are studied in order to gain estimates of the dimensions of the dried product. Studies have been conducted on volume fraction variations in the drying body, which could determine distribution of stress. It has been found that for small cakes, drying through the body is controlled by rate of mass transfer from surface. For larger cakes, there are large gradients in volume fractions throughout the body (Brown, 2003).

1.4 Purpose of this work

The purpose of this work is to determine the stability of using the Runge-Kutta fourth order method to describe particle dynamics at different time steps. In addition, the accuracy of using the numerical method with varying interparticle gradients and particle distances is also determined. Chapter 2 consists of background theory and simulation sequences. Chapter 3 contains information about the numerical method and simulations. Chapter 4 displays the results and finally, conclusions and recommendations are made in chapter 5.

CHAPTER 2

THEORY OF COLLOIDAL INTERACTIONS AND NUMERICAL METHODS

2.1 Background theory

In order to track particles and evaluate their response to perturbations introduced into the system, a study of their dynamics is performed. The motion of particles is governed by the Langevin equation, which is essentially Newton's law, but includes a stochastic term associated with Brownian motion. The Langevin equation is as given below.

$$m\frac{du}{dt} = F_H + F_p + F_B \tag{1}$$

There are 3 different forces that are taken into account: The Hydrodynamic Force, the Brownian Force and the Interparticle Force. In the overdamped limit, where the inertia of particles is negligible, the Langevin equation reduces to:

$$0 = F_H + F_p + F_B \tag{2}$$

Hydrodynamic forces:

Hydrodynamic forces have to do with the motion of colloidal particles in a viscous fluid. There are 2 aspects to hydrodynamic forces. The first is the relative motion of a tagged colloidal particle with respect to the average effect of the solvent molecules. The second is the motion of the tagged particle with respect to each of the other colloidal particles. Hydrodynamic forces are complicated to model and are characterized by a Resistance Matrix (R). Hydrodynamic forces (F^H) are linearly related to translational velocities (U) through R. Torques (T^H) are linearly related via R to the rotational velocities (Ω).

$$\begin{pmatrix} F^H \\ T^H \end{pmatrix} = -R * \begin{pmatrix} U \\ \Omega \end{pmatrix} \tag{3}$$

The resistance tensor is approximated in different ways, depending on the type of computational simulation used. It can either be vastly simplified, as is done in Brownian dynamics or complex, as is done in Stokesian Dynamics. The different types of simulation methods will be described in more detail in the next section (Russel, 1991).

Brownian forces:

Brownian forces arise from the random stochastic movement of particles. There are large differences in time and length scales between the small solvent molecules and the larger colloidal particles.

$$\langle F^B(t)\rangle = 0 \tag{4}$$

$$\langle F^B(t)F^B(t+\Delta t)\rangle = 2kT\delta_D(\Delta t)R \tag{5}$$

At any point in time, the average force on a particle is zero. In the second equation, δ_D is the dirac delta function and Δt is the difference in time between time being analyzed and viscous relaxation time of the fluid. The correlation of forces between 2 different times is given by the second equation.

Interparticle forces

Interparticle forces result from both existing and added attractions and repulsions in a system. These attractive and repulsive forces can be introduced into the system through methods such as depletion attraction and introduction of charge. Depletion attraction has to do with introducing polymer into the system and creating an unbalanced osmotic pressure, which causes particles to be pushed together. The equation for interparticle force is described as follows:

$$F_i^P = \sum_{j\neq i} -\frac{\partial V(|x_j - x_i|)}{\partial r} \tag{6}$$

The equation states that on a tagged particle i, the interparticle force is calculated as a sum of the negative derivative of the interparticle potential between the tagged particle and each of the other particles.

2.2 Types of simulation methods

Simulations depict a more ideal case of particle shearing, as opposed to experiments, in which particles tend to aggregate despite shearing. Simulation methods can broadly be classified into 2 broad categories. Methods such as Molecular Dynamics consider the effects of individual fluid particles. This makes simulations very complicated and able to depict only what happens at short time scales. Methods such as Brownian Dynamics, Stokesian Dynamics and Fast Lubrication Dynamics consider the solvent to be a continuum and consider the average effects of the solvent molecules. Therefore, these methods are not as complex and can be used to evaluate fluid dynamics at longer time scales.

The main difference in these 3 simulation methods is in how they approximate the Resistance Matrix. There are 2 components to the Resistance Matrix. The first are the far-field forces and the second are near-field forces.

$$R = R_{FF} + R_{NF} \tag{7}$$

Brownian Dynamics (BD)

In Brownian dynamics, only stokes drag through the particles is considered and effects of hydrodynamics are ignored. The far-field term is approximated as an isotropic tensor and the near-field term is ignored altogether. A simplified equation of the resistance tensor is as follows:

$$R = R_0 I + 0 \tag{8}$$

This technique has also been extended to include hydrodynamic interactions. In the study performed by Mcammon, hydrodynamic interactions were introduced through an interparticle friction tensor that was position-dependent (Bybee, 2009).

Stokesian Dynamics (SD)

Stokesian Dynamics is used to more accurately depict hydrodynamic interactions. R_{FF} is a dense matrix that describes long-range interactions using a technique called the Method of Reflections. R_{NF} is described by lubrication interactions that result from a small

viscous fluid layer that separates particles in very close proximity. These forces cause particle motion to tend to zero as they get close to each other (Brady, 1988). The far-field term, in this case, is estimated using the method of reflections.

There have also been other methods used in the approximation of the hydrodynamic interactions, including the fluid particle dynamics (Bybee, 2009) which involves the use of the Navier Stokes Equation to describe hydrodynamic interactions and smoothed profile method (Bybee, 2009), which involves the use of the Eularian-Lagrangian Method. Stokesian Dynamics is computationally intensive and involves the use of complicated math that can be difficult to apply to non-spherical particles. The equation for Stokesian Dynamics is as follows:

$$R = (R_{FF}) + (R_{LUB}) = ((I - R)^{-1}.R^{1B}) + (R^{2B} - R_{\infty}^{2B}) \quad (9)$$

Fast Lubrication Dynamics(FLD)

Fast Lubrication Dynamics is a method that is much less computationally intensive than Stokesian dynamics and shows fairly good agreement with Stokesian Dynamics up till volume fractions of 0.5. FLD is also much more accurate that Brownian Dynamics as hydrodynamic interactions are also included in calculating the resistance tensor. The Fast Lubrication Dynamics method retains lubrication interactions within a short-cutoff and includes an isotropic term to approximate far-field interactions and neglected near-field interactions. The equation for the Fast Lubrication Dynamics is as follows:

$$R = (R_{FF}) + (R_{LUB}) = (R_0 I) + \frac{1}{\delta} + log\delta \quad (10)$$

The Langevin equation often reduces to an ordinary differential equation, which is then solved using a numerical method, as will be described in the section below (Bybee, 2009).

2.3 Numerical methods

Numerical analysis consists of studying algorithms that use numerical approximation in order to solve problems in mathematical analysis. There are many types of numerical methods used, with each having its own advantages and disadvantages. The numerical

methods used to study ODEs include the Euler Method, the backward Euler method and the Runge Kutta method. These numerical methods can further be divided into explicit and implicit methods. Explicit methods use the state of a system at a current time and calculate the state at a later time. Implicit methods determine solutions using both the current and later states. It is more complicated to calculate solutions using the implicit method. However, implicit methods are best to handle stiff differential equations. (Explain stiff solutions).

The most basic explicit method is the Euler method. The Euler method is first-order. Therefore, the error at any given time is proportional to the time-step. The Euler method consists of approximating values at the next time step, by approximating it to be a value along a tangent line near the initial point. The basic equation is as follows:

$$y_{k+1} = y_k + hf(t_k, y_k) \tag{11}$$

Therefore, the time between the initial point and the next should be chosen such that the 2 solutions are close enough. A compromise needs to be made between accuracy and speed of computation needs to be made.

The backward Euler method is an implicit method. In the backward Euler method, the ODE is solved as follows:

$$y_{k+1} = y_k + hf(t_{k+1}, y_{k+1}) \tag{12}$$

As can be seen, due to the y_{k+1} term appearing on both sides of the equation, the system needs to be solved using an iteration method. The backward Euler method is also 1st order.

The Runge-Kutta methods consist of both explicit and implicit methods. The one used in this study is the 4th order Runge-Kutta method, which is an explicit method. This method is fourth order accurate. The basic equations used in this method are as follows:

$$y_{k+1} = y_k + \frac{1}{6}h(k_1 + 2k_2 + 2k_3 + k_4) \tag{13}$$

$$k_1 = f(t_k, y_k) \tag{14}$$

$$k_2 = f(t_k + \frac{1}{2}h, y_k + \frac{1}{2}hk_1) \quad (15)$$

$$k_3 = f(t_k + \frac{1}{2}h, y_k + \frac{1}{2}hk_2) \quad (16)$$

$$k_4 = f(t_k + h, y_k + hk_3) \quad (17)$$

Each value is estimated using an initial value and the weighted average of 4 increments. Each increment consists of the product between h and an estimated tangent of the function (Chapra, 2014).

Stability

Numerical solutions sometimes grow unbounded despite the exact solution not doing so. There are 3 different conditions to define the stability of a numerical method. The first is a stable numerical scheme, in which the solution does not grow unbounded despite the choice of step size. The second is the unstable numerical scheme, whereby the solution blows up despite choice of step size. In these cases, accuracy of the numerical method does not matter since they would blow up. Last, there is the conditionally stable numerical scheme, in which certain choice of parameters would cause the numerical solution to go unbounded. In order to determine which of these properties apply, stability analysis is performed.

In order to study stability, a simple ODE is considered:

$$\frac{dy}{dt} = \lambda y \; with \; y(0) = y_0 \quad (18)$$

The exact solution to this problem is:

$$y(t) = y_o e^{\lambda t} \quad (19)$$

This solution is asymptotically stable if lambda is a negative number and becomes unstable as lambda is positive and increasing.

When Euler's method is applied to this ODE, the equation becomes:

$$y_{k+1} = y_k + h\lambda y_k \quad (20)$$

When the terms are regrouped, the following equation is achieved:

$$y_{k+1} = (1 + h\lambda)^k y_o \tag{21}$$

In order to obtain stability with this equation, as k tends to infinity, we would want the following condition to be met:

$$-1 < (1 + \lambda h) < 1 \tag{22}$$

$$0 < h < \frac{2}{|\lambda|} \tag{23}$$

The stability analysis for the explicit Euler method is similar to the Rk4 method. Therefore, this is the condition that needs to be met for the case of this study.

In an equation as follows:

$$\frac{dy_i}{dt} = G(y, t) \tag{24}$$

λ is usually taken to be:

$$\lambda = \frac{dG}{dy_i} \tag{25}$$

The above method is used to conduct the stability analysis in the following chapter (Moin, 2010).

CHAPTER 3

METHOD AND RESULTS

In chapter 3, we will look at a test case used in order to determine the validity and stability of using the 4th order Runge Kutta method to illustrate particle dynamics. Additionally, the test case will also be used to illustrate how the stability analysis was conducted.

3.1 Test case

Particle dynamics are generally modeled using the Langevin equation, as described in the previous Chapter. For the purpose of this study, particle position after each time step was evaluated using the Runge-Kutta 4th order method, and compared to known particle positions in order to investigate the accuracy of using the RK4 method to determine particle dynamics. Three known displacement functions in one direction are specified:

$$x_1 = 0 \tag{26}$$

$$x_2 = h_0 + A(1 + \sin(\omega t)) \tag{27}$$

$$x_3 = -h_0 - A(1 + \sin(\omega t + \emptyset)) \tag{28}$$

At each point in time, the positions of the 3 particles were evaluated.

The velocity functions were calculated directly by differentiating each of the equations:

$$u_1 = 0 \tag{29}$$

$$u_2 = A\omega \cos(\omega t) \tag{30}$$

$$u_3 = -A\,\omega\cos(\omega t + \emptyset)) \tag{31}$$

As described in the previous section, when acceleration is considered negligible, the Langevin equation is given as follows:

$$0 = F_H + F_p + F_B \tag{32}$$

For simplification, in this study, Brownian forces will be ignored. In addition, the hydrodynamic force and the interparticle forces will be modelled as follows:

$$F_H = -R \cdot u \tag{33}$$

$$F_P = \sum_{j \neq i} \frac{\gamma}{x_i - x_j} \tag{34}$$

Finally, the equation to be solved for, using the RK4 method is:

$$0 = R\frac{dx_i}{dt} - \sum_{j \neq i} \frac{\gamma}{x_i - x_j} \tag{35}$$

To generate a known analytic solution, we assume the particle positions and velocity are as given above, and calculate an auxiliary external force field such that the Langevin equation is satisfied with the specified hydrodynamic and interparticle forces.

The external force is equated to the hydrodynamic force term and the interparticle force term, such that the force balance equates to zero. Since the displacement functions and the velocity functions are known at each time step, numerical values for the external force can be calculated.

The equation that is solved using the Runge Kutta method is then:

$$R\frac{dx_i}{dt} = \sum_{j \neq i} \frac{\gamma}{x_i - x_j} + R \cdot u - \sum_{j \neq i} \frac{\gamma}{r_{ij}} \tag{36}$$

The equation above assumes that u and r_{ij} are known numerical values. A set of 3 coupled equations for the 3 particles are solved using the RK4 method, and the numerical values for the positions at each time step are determined. These values are then compared with actual positions that are determined from substituting the value of time at each time step into the known position functions.

Non-dimensionalization:

In order to simplify the equations, the ODE is non-dimensionalized. The resistance term is equated to β. The length scale is chosen to be A, the time scale is ω. The first step in non-dimensionalization is to divide the entire ODE by β, yielding:

$$\frac{dx_i}{dt} = \sum_{j \neq i} \frac{\gamma}{\beta(x_i - x_j)} + u - \sum_{j \neq i} \frac{\gamma}{\beta r_{ij}} \tag{37}$$

Next, each of the position functions is non-dimensionalized, using

$$h^* = \frac{h^*}{A} \tag{38}$$

$$x^* = \frac{x^*}{A} \tag{39}$$

$$t^* = \frac{t}{\omega} \tag{40}$$

A new non-dimensional parameter, fp* for gamma, is introduced as well.

$$fp^* = \frac{\gamma}{\beta A^2 \omega} \tag{41}$$

The non-dimensionalized versions of the displacement functions.

$$x_1^* = 0 \tag{42}$$

$$x_2^* = h^* + (1 + \sin(t^*)) \tag{43}$$

$$x_3^* = -h^* - (1 + \sin(t^* + \emptyset)) \tag{44}$$

The non-dimensionalized velocity functions are as follows:

$$u_1^* = 0 \tag{45}$$

$$u_2^* = \cos(t^*) \tag{46}$$

$$u_3^* = -\cos(t^* + \emptyset)) \tag{47}$$

The interparticle force function is non-dimensionalized as:

$$F_P{}^* = \sum_{j \neq i} \frac{fp^*}{A * (x_i - x_j)} \tag{48}$$

Finally, the non-dimensionalized ODE to be solved is as follows:

$$\frac{dx_i{}^*}{dt^*} = \sum_{j \neq i} \frac{fp^*}{A * (x_i{}^* - x_j{}^*)} + u^* - \sum_{j \neq i} \frac{fp^*}{A * r_{ij}^*} \tag{49}$$

3.2 Stability evaluation

As explained in the previous chapter, stability limits have to be considered when using a numerical method to solve a differential equation.

We consider a simplified version of our ODE in order to analyze stability limits.

$$\frac{dx_i}{dt} = \frac{fp^*}{A(x_1 - x_2)} = G(x,t) \tag{50}$$

Where x_i can be broken down into 2 components- the mean value ($\bar{x}_i$) and the change ($\hat{x_\iota}$).

When the derivative is taken as follows, the first component goes to zero.

$$\frac{dx_1}{dt} = \frac{\cancel{d\bar{x}_1}}{\cancel{dt}} + \frac{d\hat{x_\iota}}{dt} \tag{51}$$

Thus, the resulting equation is:

$$\frac{d\hat{x_\iota}}{dt} = G_o + \frac{dG}{dx_i}\hat{x_\iota} \tag{52}$$

$$\frac{dG}{dx_i} = \frac{-fp^*}{A^*(x_1 - x_2)^2} \tag{53}$$

$$\frac{dx}{dt} = G_0 - \lambda x_i \tag{54}$$

$$\lambda = \frac{fp^*}{A^*}\left(\frac{1}{(x_1 - x_2)^2}\right) \tag{55}$$

The distance between any 2 particles is defined as h, thus making the above equation:

$$\lambda = \frac{fp^*}{A^*}\left(\frac{1}{h^{*2}}\right) \tag{56}$$

The equation above is used to derive the proportionality of the time step with fp* and h*, respectively.

The condition for stability for a first order explicit RK method is the following:

$$|1 + (\Delta t)\lambda| \leq 1 \tag{57}$$

$$-1 \leq |1 + (\Delta t)\lambda| \leq 1 \tag{58}$$

$$\Delta t < \frac{2}{\lambda} \tag{59}$$

$$\Delta t < \frac{2A(h^*)^2}{fp^*} \tag{60}$$

For higher order Runge-Kutta methods, a similar result applies with a slightly different numerical coefficient. This derivation is then used to predict the time step for stability at different h* and fp* values and compared to actual values in order to determine accuracy.

The proportionality of the time step to h^* and fp^* are as follows:

$$\Delta t \sim h^{*2} \tag{61}$$

$$\Delta t \sim \frac{1}{fp^*} \tag{62}$$

Based on the above relationship, at different time steps, the condition for h* and fp* have been predicted as below.

Table 3.1 Table displaying the predicted time steps for stability at various h* values

h^*	Predicted Δt
.316	.1
.1	.01
.0316	.001
.01	.0001

Table 3.2 Table displaying the predicted time steps for stability at various fp* values

fp^*	Predicted Δt
10	.1
100	.01
500	.002

These predictions will be compared with actual results in the next section.

3.3 Results

Convergence:

A test on convergence was conducted in order to verify that the Runge-Kutta fourth order method displayed a fourth order accuracy. For better viewing purposes, the results have also been tabulated

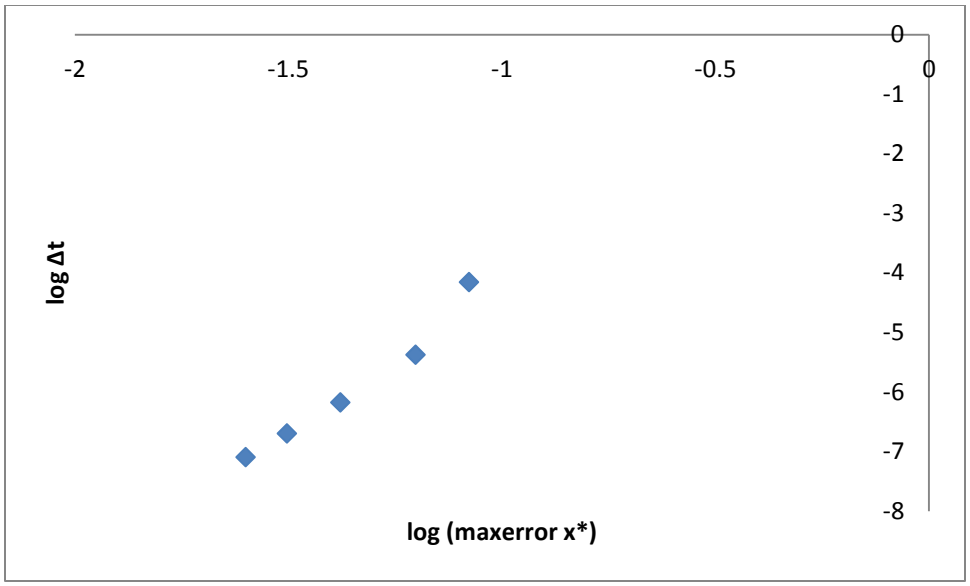

Figure 3.1 Graph displaying the fourth order convergence of Runge Kutta Fourth Error method

Table 3.3 Table displaying the fourth order convergence of Runge Kutta Fourth Error method

deltat	max error x1	max error x2	max error x3
0.025133	0	0.00000008	0.00000008
0.031416	0	0.0000002	0.0000002
0.041888	0	0.00000066	0.00000066
0.062832	0	0.00000419	0.00000419
0.083776	0	0.00006981	0.00006981

Stability:

In order to determine the stability of the fourth order methods, tests were conducted on various parameter values.

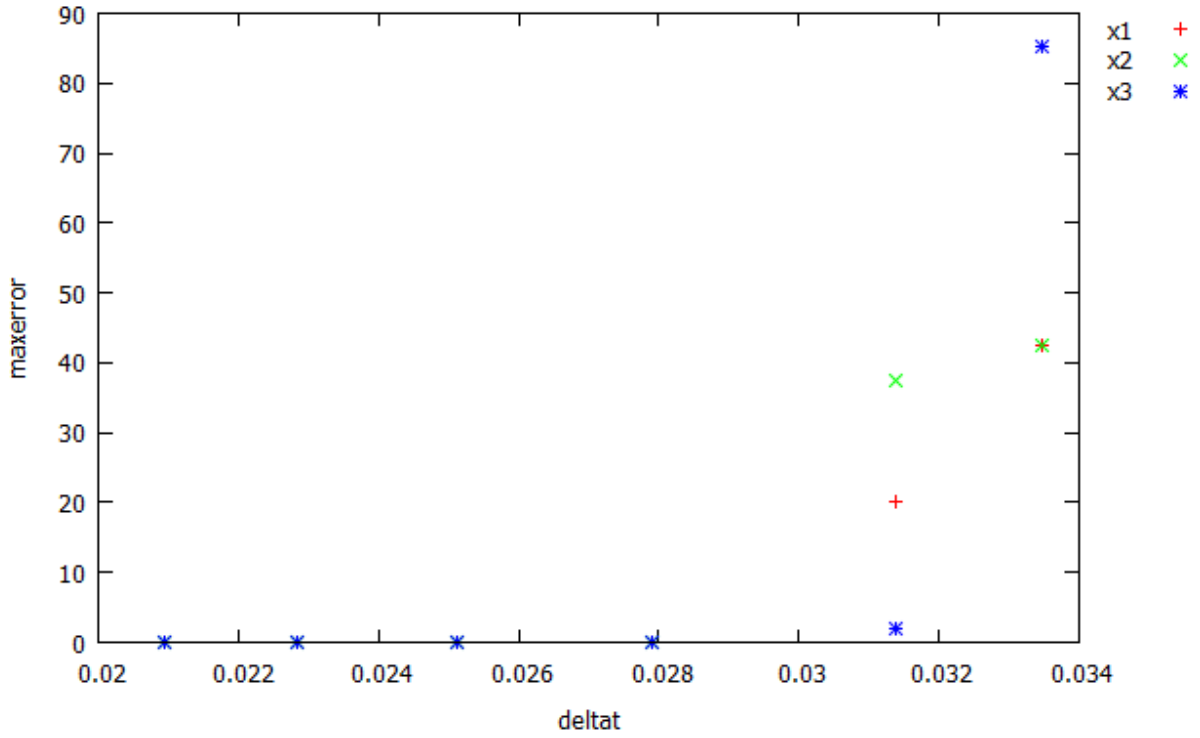

Figure 3.2 Error plot for each of the 3 particles at the following parameters: A=1, w=1, fpstar=5, phi=1, hstar=0.316.

Stability was determined to be at the time step at which the maximum error would be much higher than the average values of the time steps, as shown in the Plot 3.2. above. In this case, time steps of about 0.032 and above result in instability.

Figures 3.3 and 3.4 depict the actual locations of the 3 particles and the numerically determined locations of the 3 particles at different time steps.

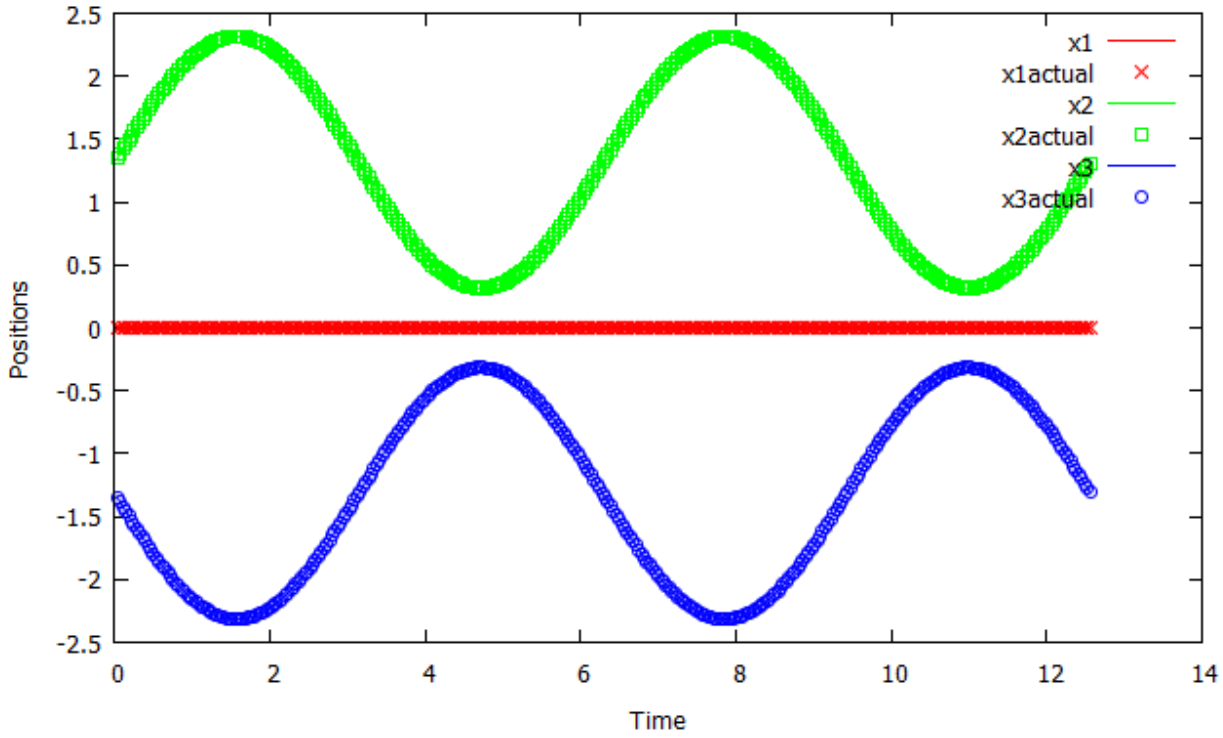

Figure 3.3 Numerical and theoretical positions for each of the 3 particles at the following parameters: A=1, w=1, fpstar=5, phi=1, hstar=0.316, deltat=0.0359 (N=350). xactual depicts the theoretical positions and x depicts the numerical positions of the particles.

At time steps smaller than that in Figure 3.3, the method is stable and there is good agreement between the actual and predicted values of the time steps.

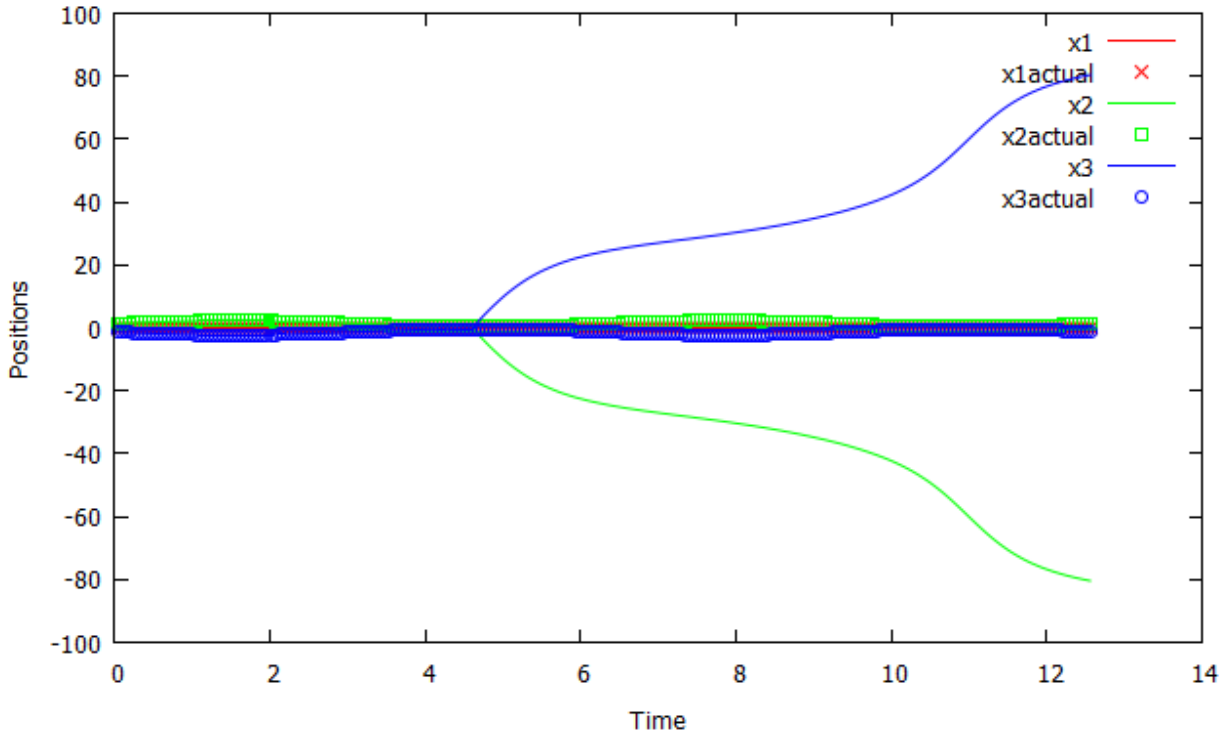

Figure 3.4 Numerical and theoretical positions for each of the 3 particles at the following parameters: A=1, w=1, fpstar=5, phi=1, hstar=0.316, deltat=0.05024 (N=250). xactual depicts the theoretical positions and x depicts the numerical positions of the particles.

As Figure 3.4 above shows, at time steps bigger than the time step used in Figure 3.3, the numerical method is unstable. The errors build up over time and there is a massive difference between actual and predicted values.

A similar analysis was conducted at various h*and fp* values. The obtained values for the time step for stability were then compared to the theoretically calculated values of the time step for stability. These results have been tabulated in Table 3.4. and Table 3.5. and graphed in Figure 3.5 and Figure 3.6.

Table 3.4 Table comparing the theoretically calculated time steps for stability against the actual time step for stability at various h* values

h*	Predicted time step	Actual time step
.316	.1	0.785398
.1	.01	0.096664
.0316	.001	0.009666

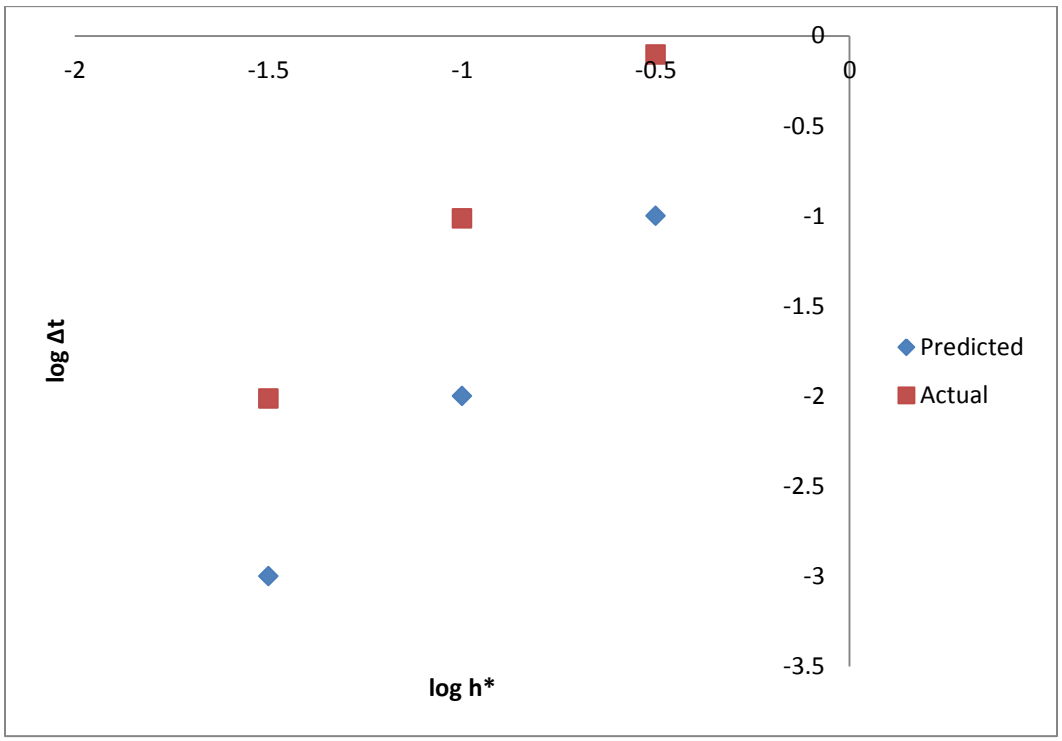

Figure 3.5 Graph comparing the theoretically calculated time steps for stability against the actual time step for stability at various h* values

Table 3.5 Comparison of the theoretically calculated time steps for stability against the actual time step for stability at various fp * values

fp*	Predicted time step	Actual time step
10	.1	0.1256
100	.01	0.011418
500	.002	0.002093

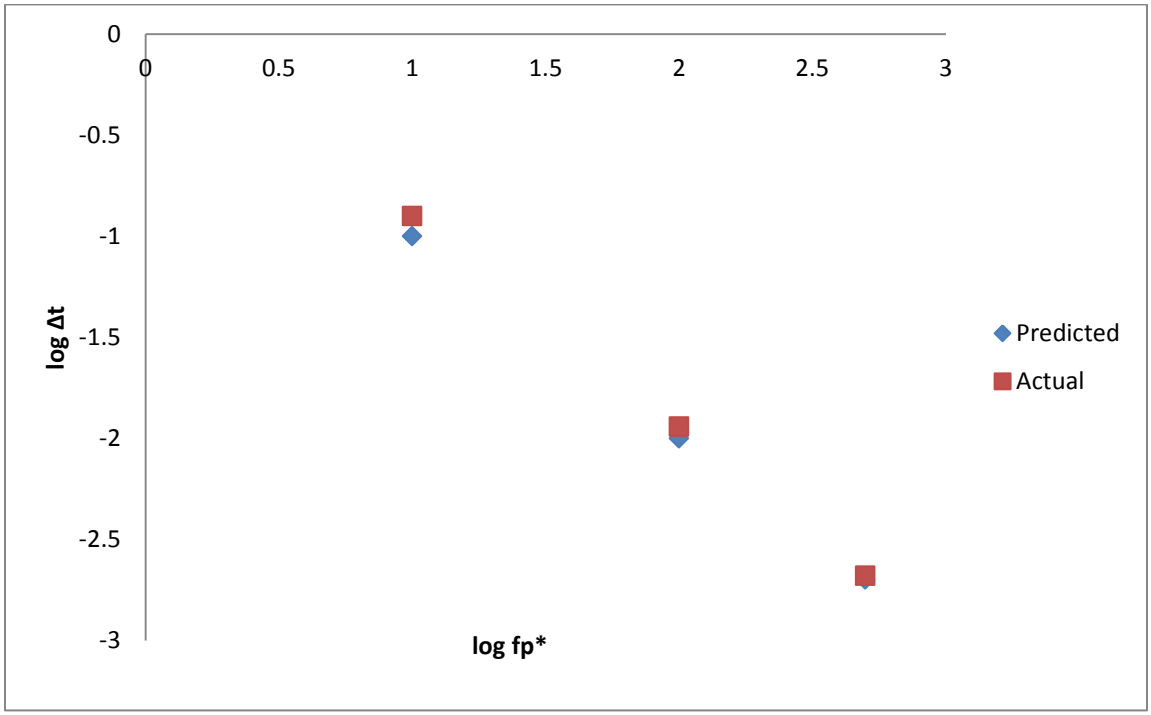

Figure 3.6 Graph comparing the theoretically calculated time steps for stability against the actual time step for stability at various fp * values

The scaling of the time step needed for stability is in excellent agreement with the predicted value. As noted above, the numerical coefficient is not expected to be identical to the prediction.

The actual and predicted results in the case of the fp* values are very close. There is very good agreement with theory, in this case.

It is important to conduct stability tests at different parameters in order to ensure that the analysis of particle dynamics is conducted accurately and does not result in large errors. It is especially important as more and more factors are included in the calculation of particle dynamics.

CHAPTER 4

CONCLUSION

Colloidal particles are of use in many different industries, including the pharmaceutical industry, the fast moving consumer goods industry, as well as in the novel microstructured materials industry. In order to cater to each of these applications, it is important to understand the interactions between colloidal particles.

The interactions were modeled using simplified hydrodynamic and interparticle forces and particle positions were determined using the 4^{th} order Runge Kutta Method. By introducing external forces as auxiliary functions, we were able to generate exact analytic solutions satisfying arbitrary hydrodynamic and interaction forces. This allowed rigorous comparison of the theoretical stability limits and the observe stability limits on time step. We found excellent agreement with the predicted and observed results.

REFERENCES

1. Brady, J., & Bossis, G. (1988). Stokesian Dynamics. *Annual Review of Fluid Mechanics, 20*, 111-157. Retrieved May 25, 2014.
2. Bybee, M. (2009). *Hydrodynamics Simulations of Colloidal Gels: Microstructure, Dynamics and Rheology*. PhD Thesis. University of Illinois at Urbana-Champaign.
3. G. M. Channell, C. F. Zukoski, "Shear and compressive rheology of aggregated alumina suspensions",*AIChE J.* **43**, 1700-1708 (1997)
4. Chapra, S., & Canale, R. (2014). *Numerical methods for engineers* (Seventh ed.).
5. Larson, R. G. (1999). *The structure and rheology of complex fluids*. New York: Oxford University Press.
6. L. A. Brown, C. F. Zukoski, "Experimental tests of two-phase fluid model of drying consolidation", *AIChE J.***49**, 362-372 (2003)
7. Moin, P. (2010). *Fundamentals of engineering numerical analysis* (2nd ed.). New York: Cambridge University Press
8. Miller, K. T., Melant, R. M. and Zukoski, C. F. (1996), *Comparison of the Compressive Yield Response of Aggregated Suspensions: Pressure Filtration, Centrifugation, and Osmotic Consolidation.* Journal of the American Ceramic Society, 79: 2545–2556.
9. S. Ramakrishnan, V. Gopalakrishnan, C. F. Zukoski, "Clustering and mechanics in dense depletion and thermal gels", *Langmuir* **21**, 9917-9925 (2005).
10. Russel, W., Saville, D., & Schowalter, W. (1991). *Colloidal dispersions*. Cambridge: Cambridge University Press.
11. S.A. Shah, S. Ramakrishnan, Y.-L. Chen, K. S. Schweizer, and C. F. Zukoski. *Scattering studies of the structure of colloid-polymer suspensions and gels.*Langmuir, 19:5128, 2003.
12. V. Gopalakrishnan, C. F. Zukoski, "Yielding behavior of thermo-reversible colloidal gels", *Langmuir* **23**, 8187-8193 (2007)
13. "The Partner for Battery Manufacturing." *Battery Manufacturing Process*. Siemens, n.d. Web. 04 June 2014.